Article

Deterministic and Probabilistic Assessment of Failure Mechanisms in Geosynthetic-Reinforced Embankments

Shen Zhang [1], Lifang Pai [2,*], Rongxue Yue [2], Yuang Shan [2] , Renjie You [2] , Yaqing Ma [2] and Xiaojuan He [2]

[1]   Seventh Branch, Zhong Qi Jiao Zhou Construction Co., Ltd., Qingdao 266000, China; 15066210707@163.com
[2]   School of Civil Engineering, Lanzhou Jiaotong University, Lanzhou 730070, China;
     17862552358@139.com (R.Y.); syangive@163.com (Y.S.); 17630403661@163.com (R.Y.);
     13893115520@163.com (Y.M.); 18153990759@163.com (X.H.)
*   Correspondence: pailifang@mail.lzjtu.cn

Abstract: Geosynthetic-reinforced embankments are subject to two primary failure mechanisms: bond failure and rupture. Bond failure occurs when the critical slip surface extends beyond the reinforced zone, while rupture occurs when the slip surface intersects the reinforcement. For a specified factor of safety and reinforcement length, there exists a minimum tensile strength of the reinforcement required to ensure bond failure only. Increasing the tensile strength beyond this minimum does not alter the failure mechanism or the factor of safety. Conversely, extending the reinforcement length while keeping the tensile strength below this critical value may lead to rupture failure at the same factor of safety. This study utilizes Monte Carlo simulation to perform a probabilistic stability analysis of these failure mechanisms in embankments with varying soil types and slope angles. The analysis evaluates safety margins in terms of the factor of safety and probability of failure. Furthermore, this study investigates the impact of cross-correlation between soil strength parameters, demonstrating that realistic values of the correlation coefficient can reduce the probability of failure for both failure mechanisms.

Keywords: embankment; geosynthetics; deterministic analysis; probabilistic analysis; stability

1. Introduction

The design of geosynthetic-reinforced embankments on soft soil traditionally relies on modified conventional deterministic limit equilibrium methods (LEMs), which have evolved to incorporate various failure mechanisms such as circular arc, log-spiral, and two-part wedge geometries [1–4]. These methods have been refined to account for the stabilizing effects of reinforcement layers intersecting potential slip surfaces, significantly bolstering the embankment's stability and resilience to external forces [5]. Despite these advancements, there remains a need for further exploration into their practical application, particularly concerning the intricate interplay between soil behaviors and the effectiveness of reinforcement strategies across different environmental conditions [6].

In practice, the primary objective of employing LEMs is to ensure the safety and durability of reinforced embankments by mitigating risks associated with reinforcement rupture and pullout failure modes. LEMs offer versatility, accommodating a wide range of embankment geometries and effectively addressing diverse geotechnical soil properties, stratigraphy variations, and dynamic loading conditions such as pore water pressures, surcharge loading, and pseudo-static seismic forces [7]. Advanced computational tools like Optum G2 play a crucial role in facilitating these complex assessments, enabling engineers to simulate and analyze potential failure scenarios with greater accuracy and efficiency [8].

However, a significant limitation of deterministic methods lies in their inability to fully capture the inherent variability of soil properties across spatial scales. This variability introduces uncertainties that can lead to discrepancies in safety assessments, underscoring the necessity for more sophisticated probabilistic approaches [9–12]. This study aims to

address this gap by employing advanced probabilistic methods, including Monte Carlo simulations, to quantitatively assess failure probabilities. Additionally, the random finite-element method (RFEM) will be utilized to evaluate the spatial variability of soil properties, providing a more comprehensive understanding of how these uncertainties impact the reliability and performance of geosynthetic-reinforced embankments [13–15].

The objective of this study is to enhance the design and safety assessment practices of geosynthetic-reinforced embankments by bridging the gap between deterministic safety factors and probabilistic reliability assessments. By integrating insights from both deterministic and probabilistic analyses, this study aims to provide actionable recommendations for improving the resilience and longevity of these critical infrastructure elements. However, achieving this goal requires a deeper understanding of soil behaviors and reinforcement interaction, which can only be achieved through advanced computational modelling and probabilistic risk assessment techniques.

2. Methods

The investigated methods encompass studies by Jewell (1996) and Rowe (2001) that explored reinforced embankments through the circular-slip method of slices approach, focusing on straightforward geometries [6,15]. Initial reinforcement designs, as established by Jewell (1991), relied on design charts employing linear and two-part wedge analyses to ensure force equilibrium [3]. These analyses identified critical reinforcement tensile strengths necessary to prevent bond failure, with failure mechanisms extending just beyond the reinforced soil mass. Interestingly, varying reinforcement tensile strengths had minimal impact on the deterministic factor of safety. However, rupture failure mechanisms, involving bond failure and rupture entirely within the reinforced soil zone, were observed when reinforcement lengths exceeded specific thresholds for given tensile strengths. The embankment's factor of safety remained consistent with a constant reinforcement length but varied with reinforcement strength. The transition between failure mechanisms highlights abrupt shifts observed between bond failure and rupture failure mechanisms, contingent upon whether the critical mechanism partially or wholly transpired within the reinforced soil zone. This underscored the sensitivity of failure modes to the spatial arrangement and strength of reinforcement materials.

Probabilistic analysis and comparison extended deterministic analyses by computing safety margins in probabilistic terms, emphasizing the greater influence of random soil property variability over reinforcement tensile strength variations on failure probabilities. Generally, bond failure mechanisms exhibited higher probabilities of failure than rupture failure mechanisms. This study expanded the scope by examining a broader array of simple geosynthetic-reinforced embankment scenarios on soft soil than earlier works by Jewell (1996) and Rowe (2001) [6,15]. Additionally, comparisons with Bathurst et al. (2007) and Sdvyzhkova et al. (2022), who applied probabilistic methods using Slide 2D software (https://www.rocscience.com/software/slide2, accessed on 8 July 2024) to assess stability and compute reliability indices for diverse design scenarios, provided additional insights [16,17]. Model validation against finite element limit analysis (FELA) results from Rowe and Li (1999) and Smith and Tatari (2016) demonstrated consistent findings, affirming the robustness of the approach despite potential differences in modelling techniques [18,19].

This comprehensive study enhances understanding and reliability in geotechnical engineering practices, providing valuable insights into reinforced embankment design. By integrating findings from Jewell (1996), Rowe (2001), and the other relevant literature, the research not only elucidates the mechanics of reinforcement failure modes but also underscores the critical role of probabilistic methods in assessing and mitigating risks [6,15]. The findings contribute to the ongoing evolution of geosynthetic-reinforced embankment design methodologies, emphasizing the need for nuanced approaches that account for both deterministic safety factors and probabilistic reliability assessments.

The accuracy of our model was validated by comparing the factor of safety (F_s) predicted using finite element limit analysis (FELA), implemented with Optum G2, with

results from the established literature. Specifically, the model was benchmarked against the finite element analysis by Rowe and Li (1999) and the FELA approach employed by Smith and Tatari (2016), ensuring robust simulation of geosynthetic behavior [18,19]. The studied embankment features a crest width of 27 m and a 2:1 slope, constructed over a 15 m thick layer of soft soil, with detailed parameters provided in Table 1. Figure 1 illustrates the impact of geosynthetic reinforcement on embankment behavior across various rupture strength scenarios. A slight elevation in results reported by Smith and Tatari (2016) compared to Rowe and Li (1999) was observed, potentially due to the upper bound nature of their solution under an associated flow rule. Our findings demonstrated excellent agreement with the results of Rowe and Li (1999), using an adequate node count and a non-associated flow rule [18,19].

Table 1. Parameter values of the reinforced embankment for validation (Rowe and Li, 1999 [18]).

Parameter	Value
Embankment crest width (W)	27
Slope gradient (n)	2
Clay layer thickness [D (m)]	15
Embankment friction angle [φ_f (°)]	37
Embankment unit weight [γ_f (kN/m^3)]	20
Soil undrained shear strength [c_s (kN/m^2)]	5–27.5
Friction coefficient at the interface (α)	1
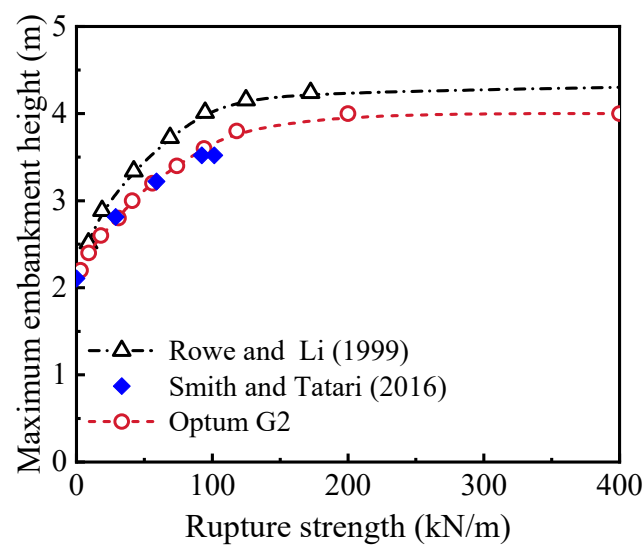
Figure 1. Maximum embankment height relative to the rupture strength of the geosynthetic (tensile force) between the current solution and findings from previous research [18,19].

The focus of this study is on the impact of soil and geosynthetic variability on a geosynthetic-reinforced embankment constructed on soft soil. The undrained shear strength of the soft soil, the rupture friction angle of the embankment, and the rupture strength are represented as a random field with a log-normal distribution (Griffiths and Fenton, 2001), mathematically expressed as follows [20]:

$$f(x) \;=\; \frac{1}{x\sigma_{lnx}\sqrt{2\pi}}exp\left[-\frac{1}{2}\left(\frac{lnx - \mu_{\ln x}}{\sigma_{lnx}^2}\right)^2\right] \tag{1}$$

where the mean $\mu_{\ln x}$ and standard deviation $\sigma_{\ln x}$ are defined as below:

$$\mu_{\ln x} = exp\left(\mu_{\ln x} + \frac{\sigma_{\ln x}^2}{2}\right) \tag{2}$$

$$\sigma_{\ln x} = \sqrt{exp(2\,\mu_{\ln x} + \sigma_{\ln x}^2)\left[exp(\sigma_{\ln x}^2) - 1\right]} \tag{3}$$

The coefficient of variation (CoV) is a dimensionless metric derived by dividing the standard deviation by the mean. This parameter quantifies the inherent variability in soil properties, allowing engineers to assess the typical and reasonable ranges of geotechnical variability [21]:

$$\text{Cov} = \frac{\sigma_{\ln x}}{\mu_{\ln x}} \tag{4}$$

In this study, the random adaptive finite element limit analysis (RAFELA) method is employed to achieve high precision in bearing capacity calculations, utilizing Optum G2 (Krabbenhoft et al., 2015) for its sophisticated handling of complex geotechnical issues [22]. The RAFELA approach involves a meticulous process of yield surface discretization through an adaptive mesh refinement strategy. This strategy dynamically adjusts mesh resolution in response to the complexity of stress and strain fields, ensuring finer resolution in regions of interest. Optum G2 is specifically chosen for its advanced RAFELA capabilities, which facilitate the handling of extensive finite element models and enable detailed probabilistic analyses. The software's integration of RAFELA allows for accurate simulation of complex geotechnical behavior. To address uncertainties associated with material properties and boundary conditions, this study conducts 1000 Monte Carlo simulations. Each simulation generates diverse input parameter sets based on probabilistic distributions, allowing for a thorough exploration of variability in bearing capacity. The adaptive meshing technique employed iteratively refines the mesh in areas with high stress gradients or intricate failure mechanisms. This iterative process ensures that the finite element model can precisely capture critical aspects of system behavior, thereby enhancing the reliability of identifying collapse mechanisms.

In this study, a parametric investigation is conducted using the geometry illustrated in Figure 1 and the parameters listed in Table 1. For a horizontal stratum of soil, the unit weight does not influence undrained collapse; thus, the weight of the soft soil is not considered. To comprehensively explore a wide range of potential parameters, the analysis utilizes the following eight independent nondimensional groups:

$$c'/\gamma H, \; c_{\text{u}}/\gamma H, \; R/\gamma H^2, \; q/\gamma H, \; H/D, \; n, \; \alpha \text{ and } \varphi'$$

The height H of the embankment serves as the normalizing parameter for the first four groups, as it has the most significant impact on stability. The assumption is made that the embankment width is adequate to prevent a central collapse mechanism. The numerical model results indicate that, for most typical parameter sets, the ratio of embankment width to soft soil thickness needs to be at least $4 + 2H/D$ to maintain the validity of this assumption. The interface coefficient α is 0.8. Separate charts are presented for different values:

(1)   Surcharge $q/\gamma H$ (0.0, 0.1);
(2)   Nondimensional undrained shear strength $c_{\text{u}}/\gamma H$ (0.155, 0.160, 0.165, 0.170);
(3)   Ratio of height of embankment and thickness of soft soil H/D (0.5, 0.75, 1.0, 1.25, 1.5);
(4)   Low or high rupture strength of reinforcement $R/\gamma H^2$ (0.1, 1.0).

3. Results

3.1. Deterministic Analysis

In deterministic analysis of geosynthetic-reinforced embankments, the stability and failure mechanisms are heavily influenced by the soil properties and geometric parameters of the embankments [19]. The study by Smith and Tatari (2016), as depicted in Figure 2,

identifies different failure mechanisms based on the type of failure slip. These mechanisms include two primary embankment failure modes and two geosynthetic failure modes, specifically bond failure and rupture. Mode 1 represents a lateral spreading failure, whereas Mode 2 corresponds to a deep-seated failure. In Mode 1, bond failure or no significant damage can occur within the geosynthetic, avoiding rupture. Conversely, Mode 2 involves the rupture of the geosynthetics, which plays a crucial role in the overall stability of the embankment, making it a more significant concern compared to Mode 1.

(a)

(b)
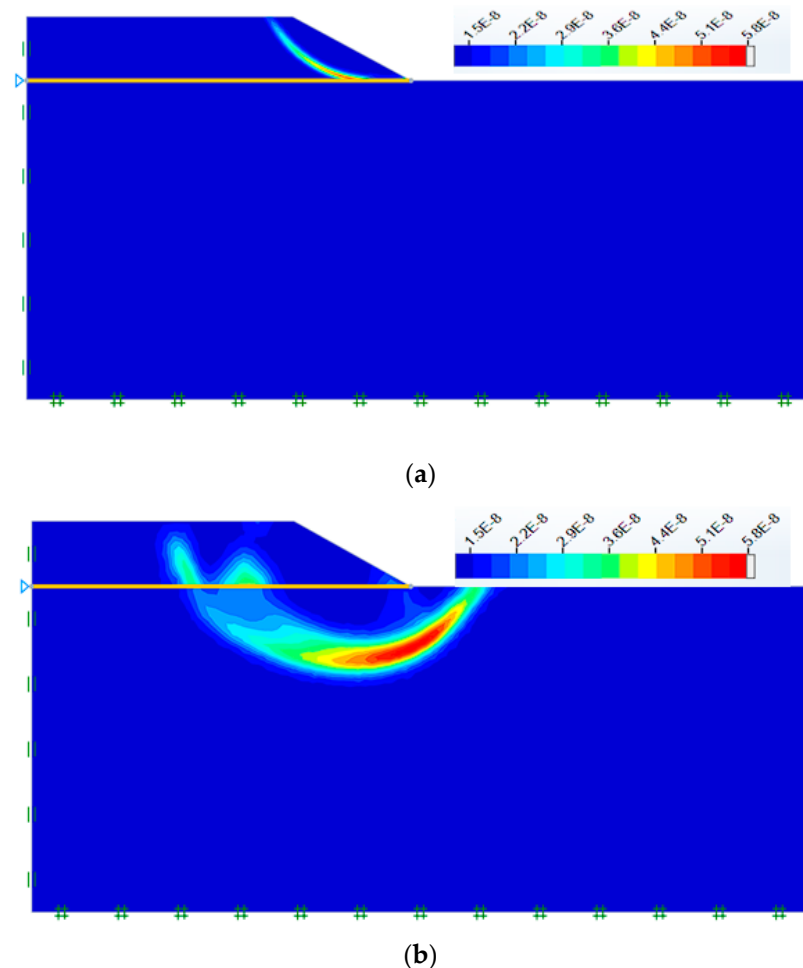
Figure 2. Failure mechanisms of the geosynthetic-reinforced embankment: (**a**) deep seated failure and (**b**) lateral spreading.

In deterministic analyses, it was observed that for a given embankment angle and a constant minimum reinforcement strength, the factor of safety (F_s) remains unchanged for reinforcement tensile strength (T) values greater than the minimum required to induce only bond failure. Additionally, for a constant minimum tensile strength equal to or lower than the threshold tensile strength necessary for rupture failure, F_s remains stable for reinforcement length values greater than the minimum needed to trigger rupture failure mechanisms [3,6]. This allows for the generation of separate contour plots of safety factors for bond failure and rupture failure mechanisms for each embankment case, providing a detailed understanding of stability under varying conditions.

The behavior of failure mechanism plots reveals that as geosynthetic tensile strength increases, the plots for rupture failure mechanisms become steeper, while those for bond failure mechanisms flatten out over their non-overlapping portions. This change in plot behavior signifies the heightened sensitivity and increased computational effort required for larger geosynthetic tensile strengths due to variations in search radii. The complexity of

these analyses necessitates more refined computational techniques to accurately capture the nuances of stability as tensile strength parameters change.

Figure 3 illustrates the transition between bond failure and rupture failure mechanisms, highlighting the presence of composite failure mechanisms. This figure demonstrates how different failure modes coexist and interact within the embankment structure. The transition is depicted through the varying tensile stresses below the minimum required for bond failure and the combinations of reinforcement tensile strength below which only rupture failure mechanisms occur. This visual representation underscores the complexity of failure behaviors, particularly as the embankment angle increases, and provides critical insights into how the stability of the embankment shifts between different types of failure mechanisms.

(a)

(b)
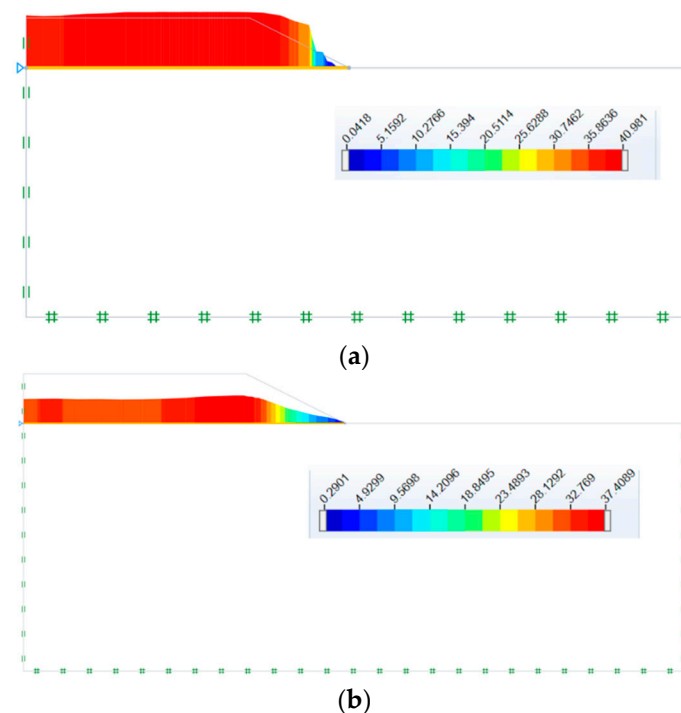
Figure 3. Failure mechanisms of geosynthetics with a geosynthetic rupture strength of 41 kN/m: (**a**) rupture and (**b**) bond failure.

Figure 4 further elucidates this by showing tensile stress values below the minimum needed for bond failure, plotting combinations of reinforcement tensile strength below which only rupture failure mechanisms occur. A pronounced transition between failure behaviors is noted with increasing embankment angle, highlighting the critical role of geometry in determining the dominant failure mechanism. This transition delineates the conditions under which the embankment shifts from one failure mode to another, providing insights into the underlying stability dynamics.

In the specific case of an embankment with a slope angle (β) of 45° ($H = 5$ m, $\gamma = 20$ kN/m^3, $\phi = 30°$, $c = 0$), the plots overlap, describing a unique locus of reinforcement length and strength that divides failure mechanisms into bond and rupture types. Corresponding factors of safety (F_s) for each plot increase with increasing geosynthetic tensile strength, indicating enhanced stability. Contour maps, as shown in Figure 5, illustrate factors of safety for this embankment case, with the upper section representing bond failure mechanisms and the lower section corresponding to rupture failure mechanisms. The boundary separating these regions aligns with the curve for $\beta = 45°$ in Figure 4 for $F_s \geq 1.1$, providing a visual representation of the interplay between reinforcement properties and embankment stability. Additionally, the minimum values of normalized reinforcement tensile strength sum $\Sigma R/(\gamma H^2)$ are plotted against the normalized cohesion of the embankment for various factors of safety. For a constant F_s, as geosynthetic

rupture strength increases, the minimum total reinforcement tensile strength needed to induce only bond failure mechanisms increases, while the minimum embankment cohesion decreases, offering a comprehensive understanding of the stability parameters involved.
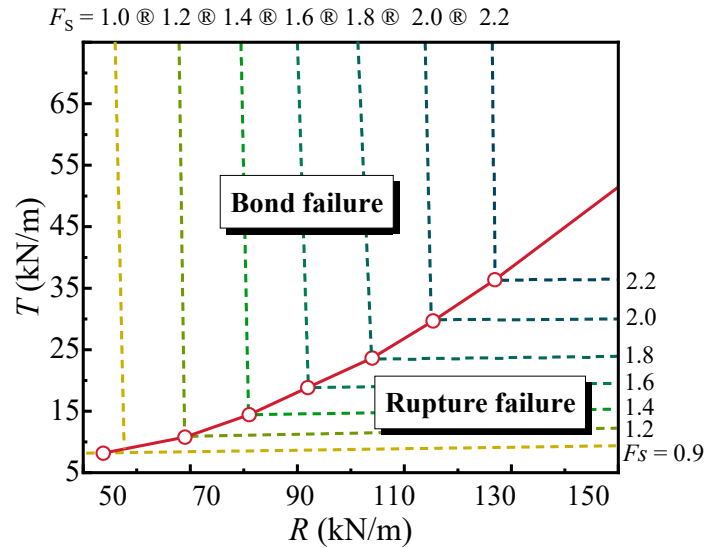
Figure 4. Factor of safety contour maps for rupture and bond failure modes with $\beta = 45°$, $H = 5$ m, $n = 4$, $\gamma = 20$ kN/m^3, $\phi = 30°$, and $c = 0$.
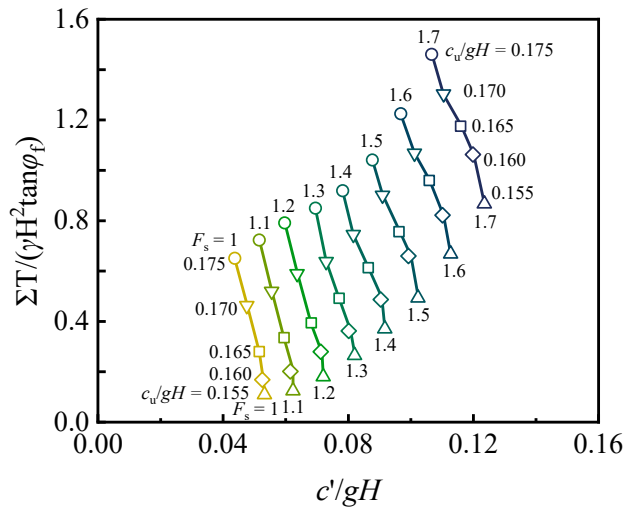
Figure 5. Relationship of reinforcement length and strength with $\beta = 45°$, $H = 5$ m, $n = 4$, $\gamma = 20$ kN/m^3, $\phi = 30°$, and $c = 0$.

3.2. Stochastic Analysis

The focus of this study is on examining the impact of soil spatial variability on the stability and failure mechanisms of geosynthetic-reinforced embankments supporting a strip footing on cohesive soil slopes. The primary aim is to understand how variations in soil properties influence embankment behavior, providing insights into the stability of reinforced embankments under different conditions. This is particularly relevant for designing more reliable and safer geotechnical structures. Previous research has highlighted the significance of geosynthetic reinforcement in improving embankment stability, but the influence of soil spatial variability has not been thoroughly investigated, making this study crucial for advancing geotechnical engineering practices.

In the baseline scenario, deterministic values were utilized for various parameters to establish a reference point. These values included unit weight ($\gamma = 20$ kN/m^3), normalized

slope height (H/D = 0.5), and slope angle (β = 1:2). By varying one parameter at a time while keeping the others constant, this study provided a clear assessment of the individual impact of each variable on the stability of the embankment. This methodical approach ensured that the effects of soil spatial variability could be accurately measured against a stable baseline, allowing for a comprehensive analysis of how different factors contribute to the overall stability of geosynthetic-reinforced embankments.

This study incorporated coefficients of variation to account for the inherent randomness in soil properties and reinforcement strength. The coefficient of variation for cohesion (COV_c) was set at 0.5, aligning with findings by Luo (2017) and Yao et al. (2023) and typical soil shear strength ranges reported by Phoon and Kulhawy (1999) [23–25]. Additionally, stationary estimates were used for the coefficient of variation of friction angle (COV_ϕ = 0.2) and cohesion (COV_c = 0.5). These values were critical for understanding the variability in soil properties and their impact on embankment stability. Stability criteria for the embankments were established, with a theoretically stable embankment having a factor of safety (F_s) of 1.0, while engineering practice recommends an F_s between 1.3 and 1.5 for safety. By adopting conservative coefficients of variation for reinforcement strength and pullout capacity, this study provided a robust framework for analyzing the reliability of geosynthetic-reinforced embankments. Reported coefficients of variation for reinforcement strength ranged from 0.01 to 0.10 and from 0.20 to 0.27 [26–28]. Bathurst et al. (2011) found that post-installation variability in geogrid tensile strength could reach COV_T = 0.2, and this study adopted a conservative COV_T = 0.15. This detailed approach ensured that the probabilistic analyses were grounded in realistic and practical assumptions, enhancing the applicability of the findings.

Random variability in reinforcement strength and pullout capacity was considered in this study's probabilistic calculations, recognizing their significant impact on failure probability. Variability in pullout capacity was treated as a function of random variability in ϕ and c. Although pullout rarely governs slope stability, conservative estimates were provided by the pullout model to ensure a comprehensive safety assessment. Mean values for cohesion (c), friction angle (ϕ), and tensile strength (T) used in probabilistic calculations were assumed to be nominal values used in deterministic analyses, treating these parameters as random variables with specified coefficients of variation (COV of 0.2 for ϕ and 0.15 for T). This probabilistic approach provided a nuanced understanding of how random variability in soil and reinforcement properties influences the stability and reliability of geosynthetic-reinforced embankments. By comparing these probabilistic analyses with deterministic results, this study highlighted the importance of considering soil spatial variability in geotechnical design and offered practical insights for improving the safety and performance of reinforced soil structures.

3.2.1. Effect of $R/\gamma H^2$

The influences of the normalized geosynthetic tensile strength $R/\gamma H^2$ on the failure probabilities are shown in Figure 6. Switching from rupture to bond failure mechanisms necessitates the use of greater geosynthetic rupture strength, provided all other parameters remain unchanged. In Figure 6, it is not immediately apparent, but the data points for rupture failure are associated with slightly greater geosynthetic rupture strengths compared to those for bond failure at the same safety factor. A small adjustment in normalized geosynthetic rupture strength, ranging from 0.5 to 0.6, is enough to shift the failure mode from bond to rupture. Although the safety factor remains virtually constant for each geosynthetic rupture strength, the disparity in the maximum probability of failure between rupture and bond mechanisms increases with greater geosynthetic rupture strengths (or higher safety factors). Furthermore, the lower curve illustrates a rapid decline in the probability of rupture failure as the geosynthetic rupture strength increases.
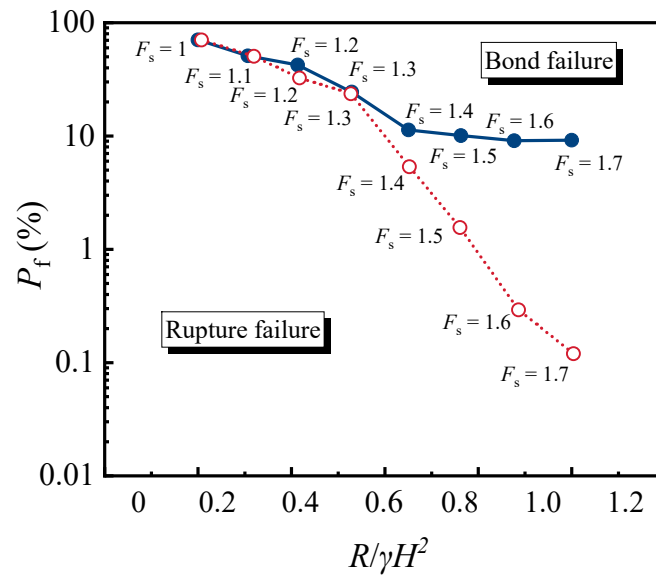
Figure 6. Probabilities of bond and rupture failure for geosynthetic-reinforced embankments as a function of geosynthetic rupture strength $R/\gamma H^2$.

Typically, the embankments are designed with a factor of safety F_s of at least 1.35 [19]. To better address this practical design range, additional analyses were performed using 1000 Monte Carlo simulations per scenario to precisely estimate the probability of failure P_f for cases with very low failure probabilities, down to 0.02%, which will be discussed in detail later. Silva et al. (2008) indicated that a P_f of 0.01% is associated with an earth dam designed with a factor of safety of 1.5, reflecting a higher-than-average engineering standard [29]. However, this 0.01% threshold is considerably lower than the probabilities depicted in Figure 7 for F_s values ranging from 1.5 to 2.2. It is crucial to emphasize that the chart represents the maximum probability of failure. In examining these results, it becomes evident that maintaining a factor of safety within the specified range significantly impacts the overall failure probabilities, underscoring the importance of rigorous design and analysis to achieve desired safety levels. This detailed probabilistic approach ensures that even scenarios with minimal failure likelihoods are thoroughly evaluated, providing a robust foundation for embankment design and safety assessment.
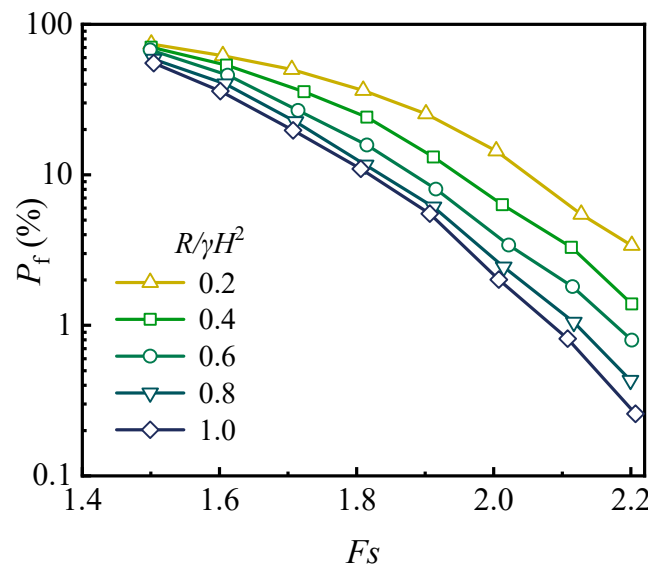
Figure 7. Effect of F_s probabilities of geosynthetic-reinforced embankments as a function of reinforcement rupture strength $R/\gamma H^2$.

Extended analysis of geosynthetic-reinforced embankments' stability and failure mechanisms reveals critical insights into the relationship between the F_s and P_f. Figure 8 extends the analysis from Figure 7, covering a range of F_s from 1.5 to 2.2 and maximum P_f values up to 20%. This broader scope allows for a detailed examination of the practical and theoretical implications of varying safety factors and failure probabilities in reinforced embankment design. Practical guidelines for geosynthetic-reinforced embankments, as delineated in the lower shaded area of Figure 8, are based on Silva et al. (2008)'s recommendations, which suggest maintaining F_s values of at least 1.5 and P_f values of no more than 0.01% [29]. Achieving these parameters necessitates specific combinations of normalized reinforcement tensile strength $R/\gamma H^2$ and high F_s. For instance, maintaining a low P_f requires relatively low normalized reinforcement tensile strength alongside higher F_s values. Conversely, for scenarios where the probability of rupture failure is considered, the P_f can be higher, as these systems, akin to other high-strength redundant soil–structure systems, can redistribute loads if a single reinforcement fails. This principle supports employing a target P_f of 1% in load and resistance factor design (LRFD) calibration for reinforced soil walls and soil nail walls, as noted by Allen et al. (2005), Bathurst (2014), and Lazarte (2011) [30–32].
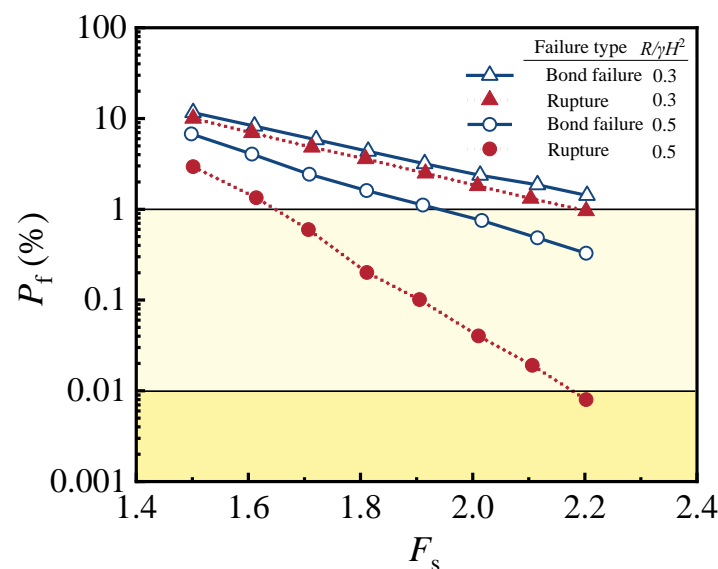
Figure 8. Highest probability of rupture failure for geosynthetic-reinforced embankment with various $R/\gamma H^2$ compared to a mean factor of safety ($1.5 \leq F_s \leq 2.2$).

The acceptance criteria for probabilities of failure in geosynthetic-reinforced embankments diverge significantly between rupture and bond failures. For bond failure, the maximum target P_f should remain below 0.01%, consistent with Silva et al. (2008)'s guidance. This conservative criterion ensures the structural integrity of geosynthetic-reinforced embankments under typical load conditions [33]. In contrast, for rupture failure limit states, a higher P_f of 1% is deemed acceptable, as illustrated by the upper line in Figure 8. This higher threshold is justified by the system's ability to maintain overall stability despite the failure of individual reinforcement elements, reflecting the redundancy and robustness inherent in the design of geosynthetic-reinforced systems.

In summary, Figure 8 illustrates the nuanced approach required in evaluating the stability and failure mechanisms of geosynthetic-reinforced embankments. The balance between F_s and P_f, particularly in the context of bond and rupture failures, underscores the importance of tailored design criteria. Achieving optimal stability involves carefully calibrating reinforcement tensile strength and safety factors to meet the specified failure probability targets, ensuring both practical and theoretical design requirements are satisfied.

3.2.2. Effect of H/D

Figure 9 presents the impact of normalized embankment height H/D on failure probabilities. When transitioning from bond failure to rupture failure mechanisms, an increase in H/D is necessary, assuming all other parameters remain constant. While this transition is subtle in Figure 9, it is evident that the data points for rupture failure correspond to slightly higher geosynthetic rupture strengths than those for bond failure at the same factor of safety. A small increase in normalized embankment height, typically between 1.3 and 1.5, can effectively switch the failure mechanism from bond to rupture. Despite the factor of safety remaining nearly constant for each geosynthetic rupture strength, the maximum probability of failure for rupture mechanisms diverges significantly from that of bond mechanisms as the embankment height (or safety factor) increases. This indicates that while both failure types are influenced by the same geosynthetic parameters, rupture failures become less probable with a larger height of the embankment. Furthermore, the lower curve in Figure 9 highlights a pronounced decline in the probability of rupture failure as the embankment height increases, underscoring the effectiveness of higher embankment height in mitigating rupture failures.
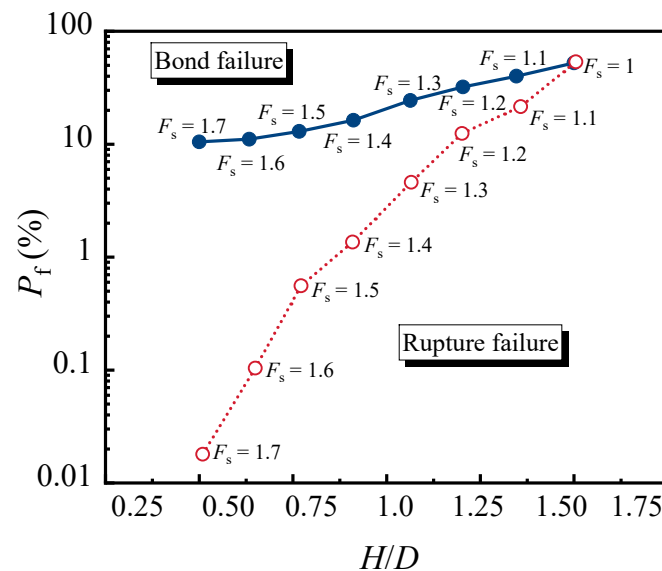
Figure 9. Probabilities of bond and rupture failure for geosynthetic-reinforced embankments as a function of normalized embankment height.

Figure 10 extends the analysis from Figure 9 to cover a factor of safety F_s range of 1.5 to 2.2 and maximum probability of failure P_f values up to 20%, akin to Figure 7. The 0.01% threshold is significantly lower than the probabilities shown in Figure 10 for F_s values between 1.5 and 2.2. It is important to highlight that the chart displays the maximum probability of failure. Analyzing these results reveals that maintaining a factor of safety within the specified range greatly influences overall failure probabilities. This underscores the critical need for meticulous design and analysis to achieve the desired safety levels. By adopting this comprehensive probabilistic approach, even scenarios with minimal failure likelihoods are thoroughly assessed, ensuring a solid foundation for embankment design and safety evaluation. The inclusion of different embankment heights highlights the adaptability and precision of the probabilistic approach, making it a valuable tool for optimizing embankment stability and safety in diverse geotechnical conditions.
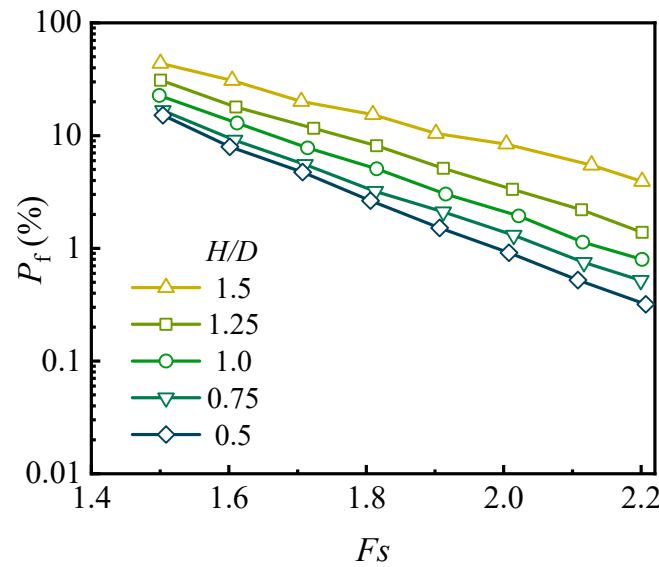
Figure 10. Probabilities of embankment collapse for geosynthetic-reinforced embankments as a function of normalized embankment height, H/D.

Figure 11 illustrates that achieving maximum probabilities of failure within the practical ranges ($F_s \geq 1.5$ and $P_f \leq 0.01\%$) requires combinations of relatively low embankment height and high F_s. Higher probabilities of failure (P_f up to 1%) may be acceptable for rupture failure in geosynthetic-reinforced embankments, achievable with lower F_s and higher normalized embankment height compared to the 0.01% criterion. Consequently, while both rupture and bond failures are significant, the acceptance criteria for their probabilities of failure differ, reflecting their respective impacts on the structural integrity of geosynthetic-reinforced embankments.
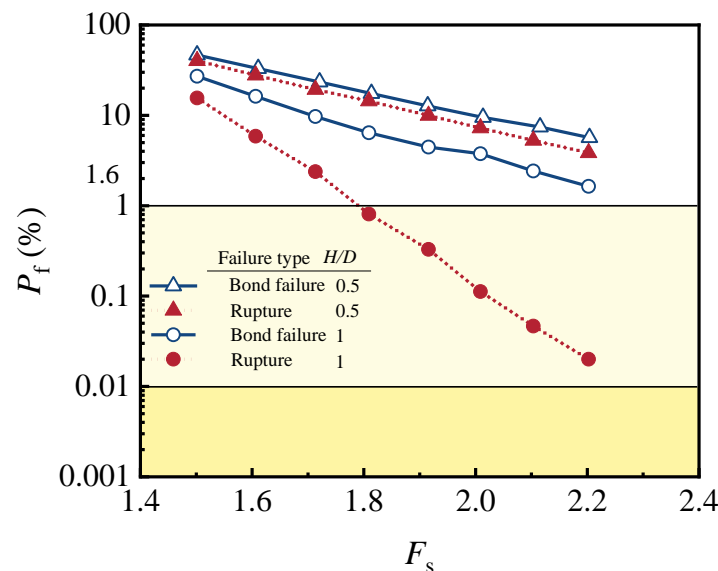
Figure 11. Highest probability of rupture failure for geosynthetic-reinforced embankment with various H/D compared to mean factor of Safety ($1.5 \leq F_s \leq 2.2$).

3.2.3. Effect of $c_u/\gamma H$

Figure 12 illustrates the effect of normalized undrained shear strength of the soft soils $c_u/\gamma H$ on failure probabilities. To shift from rupture failure to bond failure mechanisms, an increase in $c_u/\gamma H$ is necessary while keeping all other parameters constant. Although this transition is subtle in Figure 12, it is clear that the data points for rupture failure align

with slightly higher geosynthetic rupture strengths compared to those for bond failure at the same factor of safety. A modest increase in normalized undrained shear strength of the soft soil, typically between 1.575 and 1.6, can effectively alter the failure mechanism from bond to rupture. Even though the factor of safety remains nearly constant for each undrained shear strength, the maximum probability of failure for rupture mechanisms differs significantly from that of bond mechanisms as the undrained shear strength (or safety factor) increases. This suggests that while both failure types are influenced by the same geosynthetic parameters, rupture failures become less likely with lower undrained shear strength. Additionally, the lower curve in Figure 12 demonstrates a marked decrease in the probability of rupture failure as the undrained shear strength increases, highlighting the effectiveness of greater shear strength in reducing rupture failures.
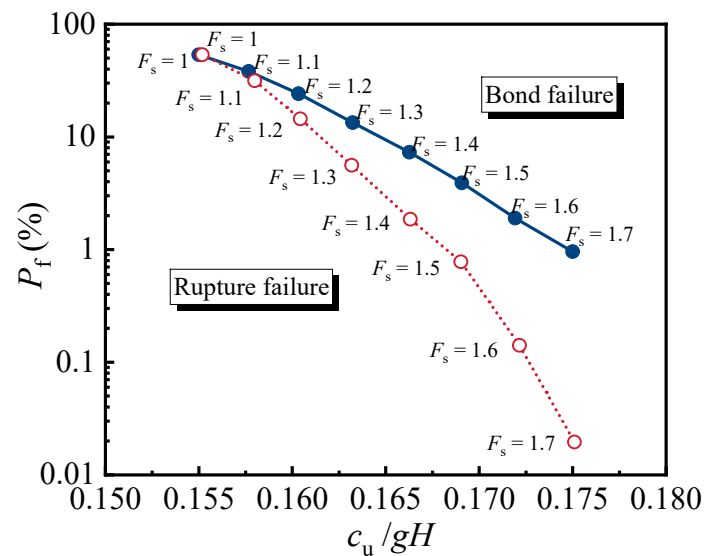
Figure 12. Probabilities of bond and rupture failure for geosynthetic-reinforced embankments as a function of the undrained strength of clay.

Figure 13 examines a factor of safety F_s range of 1.5 to 2.2 and maximum failure probabilities P_f up to 20%. The 0.01% threshold is notably lower than the failure probabilities presented for F_s values between 1.5 and 2.2. This figure specifically illustrates the peak failure probabilities, underscoring that maintaining an F_s within this specified range profoundly impacts overall failure probabilities. These findings underscore the importance of precise and thorough design and analysis to achieve desired safety margins. By employing this detailed probabilistic methodology, scenarios with very low failure likelihoods are also rigorously evaluated, ensuring a strong foundation for embankment design and safety assurance. The analysis's inclusion of various shear strengths of soft soil further highlights its adaptability and precision, making it an invaluable approach for optimizing embankment stability and safety across different geotechnical scenarios.

Figure 14 reveals that to achieve maximum probabilities of failure within the practical limits, combinations of relatively low shear strength and high factors of safety are necessary. It is noted that for rupture failures in geosynthetic-reinforced embankments, higher failure probabilities may be considered acceptable. These higher probabilities can be attained with lower F_s and increased normalized shear strength compared to the stringent 0.01% failure probability criterion. This differentiation underscores the varying acceptance thresholds for rupture and bond failures, highlighting their distinct impacts on the structural integrity of geosynthetic-reinforced embankments. By recognizing the different probabilistic thresholds for these failure modes, engineers can better tailor their design and safety evaluations to ensure robust and reliable embankment performance across diverse conditions. This approach not only enhances the understanding of failure mechanisms but also supports the development of optimized reinforcement strategies to mitigate potential risks effectively.
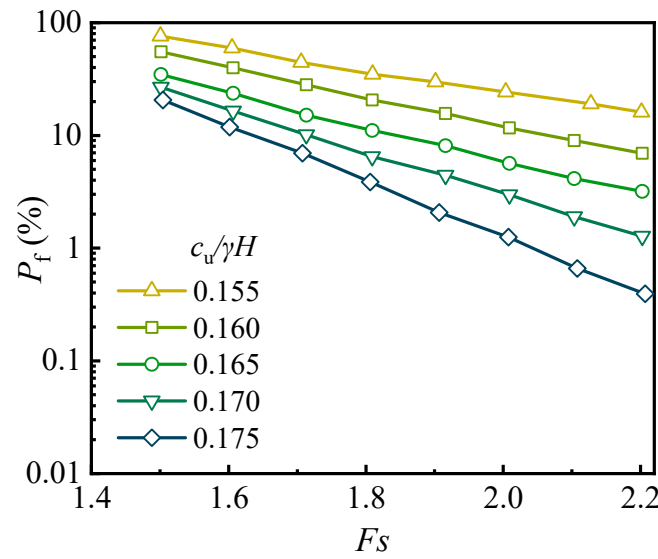
Figure 13. Effect of probabilities for geosynthetic-reinforced embankments as a function of normalized undrained shear strength.
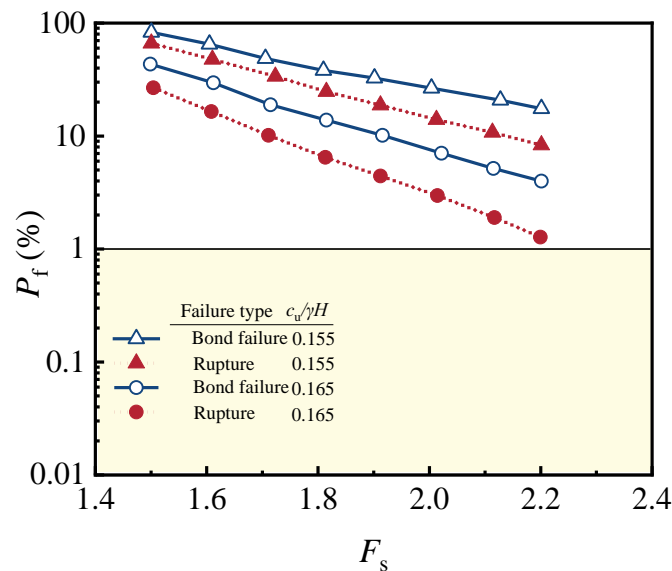
Figure 14. Highest probability of rupture failure for geosynthetic-reinforced embankment with various $c_u/\gamma H$ compared to mean factor of safety ($1.5 \le F_s \le 2.2$).

4. Conclusions

This study presents a novel probabilistic stability analysis of geosynthetic-reinforced embankments using Monte Carlo simulations and a random adaptive finite element limit analysis (RAFELA) implemented through Optum G2. The innovative aspect of this research lies in its comprehensive examination of two primary failure mechanisms—bond failure, where critical slip surfaces extend beyond the reinforced zone, and rupture mechanisms, where slip surfaces intersect the reinforcement layers. By investigating the transition to composite mechanisms for steep slopes, this study provides new insights into the probabilistic behavior of these systems under varying conditions.

Key findings from the analysis reveal several novel contributions: Firstly, the research identifies critical thresholds for reinforcement tensile strength, embankment height, and undrained shear strength required to ensure bond failure mechanisms. For tensile strengths above these thresholds, the factor of safety (F_s) and probability of failure remain unchanged. Secondly, it is shown that increasing reinforcement length while maintaining or reducing

tensile strength can shift the failure mechanism from bond to rupture, without affecting the F_s. This finding is crucial for optimizing reinforced embankment designs to balance safety and performance effectively.

This study also introduces probabilistic stability charts that offer conservative maximum failure probabilities and establish a link between conventional safety factors and failure probabilities. These charts serve as practical tools for geotechnical engineers, providing valuable insights and preliminary probabilistic design guidelines for geosynthetic-reinforced embankments. Furthermore, the analysis underscores the minimal impact of soil spatial variability on the reliability of probabilistic models, highlighting the critical role of proper construction practices.

In conclusion, this research advances the understanding of reinforcement effects on embankment stability by integrating RAFELA with Monte Carlo simulations, offering new perspectives on failure mechanisms and probabilistic design. These contributions enhance the safety and efficiency of geotechnical engineering practices and provide a robust framework for the preliminary design of geosynthetic-reinforced embankments.

Author Contributions: S.Z. mainly completed experimental data analysis, manuscript writing, and figure production. L.P., R.Y. (Rongxue Yue), Y.S., R.Y. (Renjie You), Y.M. and X.H. mainly completed the numerical calculation and manuscript verification. All authors have read and agreed to the published version of the manuscript.

Institutional Review Board Statement: Not applicable.

Informed Consent Statement: Not applicable.

Data Availability Statement: All data, models, or code that support the findings in this study are available from the corresponding author upon reasonable request.

Conflicts of Interest: Author Shen Zhang was employed by the Seventh Branch, Zhong Qi Jiao Zhou Construction Co., Ltd. The authors declare that this study received funding from China Railway Co., Ltd. The funder was not involved in the study design, collection, analysis, interpretation of data, the writing of this article or the decision to submit it for publication. The remaining authors declare that the research was conducted in the absence of any commercial or financial relationships that could be construed as a potential conflict of interest.

References

1. Der, B.S.; Ke, J.C. Modelling variability and uncertainty of geotechnical properties for reliability-based design. In Proceedings of the 9th International Conference on Soil Mechanics and Foundation Engineering, Tokyo, Japan, 10–15 July 1977; pp. 473–476.
2. Sudret, B.; Der Kiureghian, A. *Stochastic Finite Element Methods and Reliability: A State-of-the-Art Report*; Department of Civil and Environmental Engineering, University of California: Berkeley, CA, USA, 2000; pp. 18–34.
3. Jewell, R.A. Application of revised design charts for steep slopes. *Geotext. Geomembr.* **1991**, *10*, 203–233. [CrossRef]
4. Bathurst, R.J.; Allen, T.M.; Walters, D.L. Analysis of installation damage for geogrids used in reinforced soil walls. *J. Geotech. Geoenviron.l Eng.* **2011**, *137*, 139–145. [CrossRef]
5. Guo, Y.; Jiang, S.H.; Zhou, C.B.; Zhang, L.M. Three-dimensional slope reliability analysis considering spatial variability of soil properties. *Eng. Geol.* **2019**, *259*, 105175. [CrossRef]
6. Jewell, R.A. *Soil Reinforcement with Geotextiles. CIRIA Special Publication 123*; Thomas Telford Publishing: London, UK, 1996; pp. 1–102.
7. Ali, A.; Lyamin, A.V.; Huang, J.; Li, J.H.; Cassidy, M.J.; Sloan, S.W. Probabilistic stability assessment using adaptive limit analysis and random fields. *Acta Geotech.* **2017**, *12*, 937–948. [CrossRef]
8. Shen, S.L.; Karakus, M. Evaluation of soil-geosynthetic interaction using experimental and numerical methods. *Geotext. Geomembr.* **2014**, *42*, 52–61.
9. Cho, S.E.; Park, H.C. Effect of spatial variability of soil properties on the stability of a two-layer slope using a random finite element method. *Comput. Geotech.* **2010**, *37*, 187–194. [CrossRef]

10. Saik, P.; Rysbekov, K.; Kassymkanova, K.K.; Lozynskyi, V.; Kyrgizbayeva, G.; Moldabayev, S.; Salkynov, A. Investigation of the rock mass state in the near-wall part of the quarry and its stability management. *Front. Earth Sci.* **2024**, *12*, 1395418. [CrossRef]

11. Javankhoshdel, S.; Bathurst, R.J. Reliability-based analysis of soil slopes reinforced with geosynthetics. *Geotext. Geomembr.* **2014**, *42*, 275–290. [CrossRef]

12. Bathurst, R.J.; Miyata, Y. Reliability-based design for geosynthetic reinforcement considering installation damage and creep. *Geotech. Eng. J.* **2015**, *45*, 67–78. [CrossRef]

13. Pan, Q.; Dias, D.; Soubra, A.H. Probabilistic analysis of the stability of rock slopes using the response surface method. *Comput. Geotech.* **2019**, *114*, 103133. [CrossRef]

14. Luo, N.; Bathurst, R.J. Probabilistic analysis of geosynthetic-reinforced soil walls. *Can. Geotech. J.* **2017**, *54*, 307–321. [CrossRef]

15. Rowe, R.K. Geosynthetics and the minimization of contaminant migration through barrier systems beneath solid waste. In Proceedings of the 6th International Conference on Geosynthetics, Atlanta, GA, USA, 25–29 March 2001; Volume 4, pp. 27–56.

16. Bathurst, R.J.; Huang, B.; Allen, T.M. Reliability Analysis of Geosynthetic Reinforced Soil Walls. *Geosynth. Int.* **2007**, *14*, 178–189. [CrossRef]

17. Sdvyzhkova, O.; Moldabayev, S.; Başçetin, A.; Babets, D.; Kuldeyev, E.; Sultanbekova, Z.; Issakov, B. Probabilistic assessment of slope stability at ore mining with steep layers in deep open pits. *Min. Miner. Depos.* **2022**, *16*, 11–18. [CrossRef]

18. Rowe, R.K.; Li, A.L. Reinforced embankments over soft foundations under undrained and partially drained conditions. *Geotext. Geomembr.* **1999**, *17*, 129–146. [CrossRef]

19. Smith, C.C.; Tatari, A. Limit analysis of reinforced embankments on soft soil. *Geotext. Geomembr.* **2016**, *44*, 504–514. [CrossRef]

20. Griffiths, D.V.; Fenton, G.A. Bearing capacity of spatially random soil: The undrained clay prandtl problem revisited. *Geotechnique* **2001**, *51*, 351–359. [CrossRef]

21. Ching, J.; Phoon, K.K.; Chen, Y. Improving efficiency of random finite element method in reliability-based design by response surface approach. *Comput. Geotech.* **2016**, *78*, 77–91. [CrossRef]

22. Krabbenhoft, K.; Lyamin, A.; Krabbenhoft, J. Optum computational engineering (OptumG2). *Comput. Softw.* **2015**, 1–156.

23. Luo, N.; Bathurst, R.J. Probabilistic analysis of reinforced soil walls using random finite element method. *Comput. Geotech.* **2017**, *85*, 79–94. [CrossRef]

24. Yao, N.; Deng, X.; Luo, B.; Oppong, F.; Li, P. Strength and failure mode of expansive slurry-inclined layered rock mass composite based on Mohr–Coulomb criterion. *Rock Mech. Rock Eng.* **2023**, *56*, 3679–3692. [CrossRef]

25. Phoon, K.K.; Kulhawy, F.H. Characterization of geotechnical variability. *Can. Geotech. J.* **1999**, *36*, 612–624. [CrossRef]

26. Ferreira, J.M.; Palmeira, E.M.; Ehrlich, M. Influence of soil and reinforcement properties on the behaviour of reinforced soil walls. *Geotext. Geomembr.* **2016**, *44*, 592–603. [CrossRef]

27. Kitch, W.A.; Benson, C.H.; Bosscher, P.J. Analysis of geosynthetic-reinforced embankments over soft soil. *J. Geotech. Geoenvironmental Eng.* **2011**, *127*, 161–168. [CrossRef]

28. *JTG D30-2015*; Specifications for Design of Highway Subgrades. Ministry of Transport of the People's Republic of China (MOT): Beijing, China, 2015; pp. 1–203. (In Chinese)

29. Zerradi, Y.; Souissi, M.; Larabi, A. Application of the deterministic block theory to the slope stability design of an open-pit mine in Morocco. *Min. Miner. Depos.* **2023**, *17*, 53–60. [CrossRef]

30. Silva, F.; Brandl, H.; Schleicher, M. Risk and reliability in geotechnical engineering. In Proceedings of the 4th Asian Regional Conference on Geosynthetics, Shanghai, China, 17–20 June 2008; pp. 1–306. [CrossRef]

31. Allen, T.M.; Bathurst, R.J.; Holtz, R.D.; Lee, W.F.; Walters, D.L. A new working stress method for prediction of reinforcement loads in geosynthetic walls. *Geosynth. Int.* **2005**, *12*, 178–199. [CrossRef]

32. Bathurst, R.J. Geosynthetic-reinforced soil retaining walls and slopes: Performance and prediction. *Geosynth. Int.* **2014**, *21*, 88–103. [CrossRef]

33. Lazarte, C.A. *Soil Nail Walls Reference Manual (Report No. FHWA-NHI-10-024)*; Federal Highway Administration: Los Angeles, CA, USA, 2011; pp. 1–106.